Theor Appl Climatol
DOI 10.1007/s00704-010-0260-4

ORIGINAL PAPER

Circumglobal teleconnection and early summer rainfall in the US Intermountain West

Shih-Yu Wang · Lawrence E. Hipps · Robert R. Gillies · Xianan Jiang · Alan L. Moller

Received: 17 September 2009 / Accepted: 17 January 2010

Abstract Physical processes responsible for the abnormally wet condition in the Central Intermountain West (CIW) of the United States in June 2009 were investigated. It was illustrated that persistent rainy conditions over the CIW during June 2009 were associated with a pronounced circumglobal teleconnection pattern, which is characterized as a short Rossby wave train along the jet stream waveguide with a wave number 5 structure. The ascending motion and moisture flux convergence over the CIW associated with the cyclonic action center over the US West Coast in the teleconnection wave train could be essential for the persistent local rainfall during June 2009. Further analysis suggested that the June 2009 circulation pattern is consistent with a prevailing mode of the summer circumglobal teleconnection pattern. The findings in this study provide information for improved understanding of the early summer rainfall regime in the CIW.

1 Introduction

June 2009 was an abnormally wet month for the Central Intermountain West (CIW) of the United States. Areas of Utah and Idaho, for example, received over 400% of their climatological June rainfall (Fig. 1a). Consecutive rainfall events combined with seasonal snowmelt prolonged spring runoff and triggered mudslides along many river basins in the region. Affected by the anomalous precipitation of June 2009, Utah State University (USU; station ID 425186) in Logan, Utah recorded 3.38 in. of rain making it the eighth wettest June in its 115-year period of record. During the same month, some stations in northern Utah and southern Idaho broke records. For example, Pocatello, Idaho (station ID 107211; 120 km north of USU) received 4 in. of rain in contrast to its long-term mean of just 1 in.[1] Climatologically, precipitation in the CIW belongs to a cold season regime with a spring peak. A rapid transition in precipitation characterizes June from the wettest month of May to the driest month of July (Wang et al. 2009c). While a wet June prolongs the CIW's spring rainfall into summer, a dry June can shorten the rainy season and reduce the agriculturally important runoff through the dry season.

The atmospheric circulation over North America also undergoes considerable changes in June, including the rapid northward shift of the jet stream (e.g., Higgins et al. 1997). From April to June, a synoptic-scale trough develops over the southwest United States, deepens, and then migrates to the West Coast. The trough eventually merges with the large-scale oceanic trough over the North Pacific in July (cf. Fig. 7 of Wang and Chen 2009). The development of this spring trough over the West Coast brings in moisture and energizes local synoptic disturbances moving across the

S.-Y. Wang (✉) · R. R. Gillies · A. L. Moller
Utah Climate Center, Utah State University,
4825 Old Main Hill,
Logan, UT 84322-4825, USA
e-mail: simon.wang@usu.edu

L. E. Hipps · R. R. Gillies
Department of Plants, Soils, and Climate, Utah State University,
Logan, UT, USA

X. Jiang
Joint Institute for Regional Earth System Science & Engineering,
University of California,
Los Angeles, CA, USA

[1] Historical records of the Cooperative Observer Program (COOP) stations in the Western United States can be accessed from the Utah Climate Center webpage at http://climate.usurf.usu.edu/reports/dynamic.php.

Published online: 09 February 2010

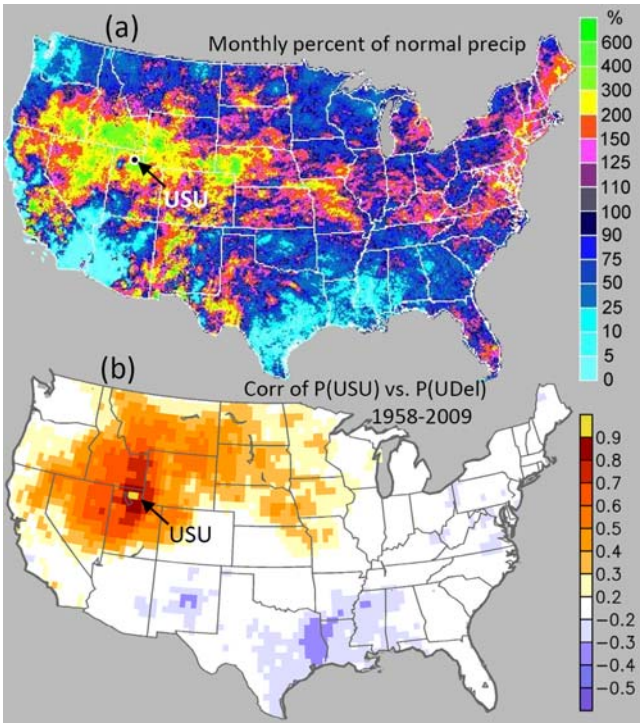

Fig. 1 **a** Monthly percent of normal precipitation in June 2009 obtained from the Advanced Hydrologic Prediction Service of National Weather Service (http://water.weather.gov/) and **b** correlation map of UDel precipitation with the USU precipitation from 1958 to 2009. The location of USU is indicated by a *dot* in **a** and the *yellow box* in **b**

CIW. In June 2009, however, this trough deepened more than expected and was embedded in a series of trough/ridge systems spanning the globe, as shown in the monthly mean streamlines at 250 hPa (Fig. 2b). The longitude–time evolution of geopotential height at 250 hPa (Fig. 2a) reveals that the trough/ridge systems developed in late May and became quasistationary through most of June. Persistent rainfall was produced in the cyclonic vorticity advection region of each trough (i.e., to the east of the troughs), including one such region in the CIW.

Recurrent short-wave patterns have been found to characterize the interannual variation of midlatitude circulations affecting North American climate (e.g., Barnston and Livezey 1987; Yang et al. 2002; Weaver and Nigam 2008). During strong El Niño-Southern Oscillation (ENSO) winters, midlatitude short-wave trains across the North Pacific are recognizable features (Chen 2002), in addition to the long-wave Pacific–North American pattern (PNA; Wallace and Gutzler 1981). Branstator (2002) identified the *circumglobal teleconnection* with a zonal wave number 5 structure that was trapped in the wintertime jet stream "waveguide." Ding and Wang (2005) further showed that the circumglobal teleconnection pattern is similarly pronounced in summer, but its timing and spatial phase are noticeably different in each month from June to September. Numerous studies (e.g., Takaya and Nakamura 2001; Lau and Weng 2002; Lau et al. 2004) have found that climate variations in Asia/Western Pacific and North America may be linked through substantial short-wave trains. The pronounced waveform circulation pattern in June 2009 (Fig. 2a, b) also suggests a possible link between the CIW precipitation variation and the summer circumglobal teleconnection. The present study examines such a link. In the following text, the terms "circumglobal teleconnection" and "short-wave train" will be used interchangeably.

2 Data

The meteorological data were obtained from both the National Centers for Environmental Prediction (NCEP) Global Reanalysis (Kalnay et al. 1996) and the ERA-40 Global Reanalysis (Uppala et al. 2005) with a 2.5° resolution for 1958–2009. As the ERA-40 data are only available up to 2002, the years2003–2009 were implemented by the newer ERA-Interim Reanalysis (Uppala et al. 2008), hereafter ERA. Precipitation data included the gauge-based monthly precipitation of the University of Delaware (UDel; Legates and Willmott 1990) at a 0.5° resolution for the time period of 1900–2008, the Global Precipitation Climatology Project (GPCP; Huffman et al. 1997) derived from rain gauge and satellite observations at a 2.5° resolution for 1979–2008, and the 3-h National Oceanic and Atmospheric Administration (NOAA) Climate Prediction Center (CPC) Morphing Technique (CMORPH; Joyce et al. 2004) precipitation derived from various microwave satellite sources with a 0.25° resolution for 2009. Because the USU station has maintained a stable observation for over a century, monthly gauge precipitation recorded at USU was also used. The correlation map of June precipitation between USU and UDel (Fig. 1b) during the time period of 1958–2009 depicts a regional pattern similar to that in 2009 (Fig. 1a). Thus, the USU precipitation records are considered representative of the CIW rainfall variability.

3 Results

The normal mode of the circumglobal teleconnection (i.e., climatic stationary short-wave train; Chen 2002) in June can be depicted by the long-term mean (1958–2008) geopotential height spatially filtered with zonal wave numbers 5 and greater, using harmonic analysis. This wave

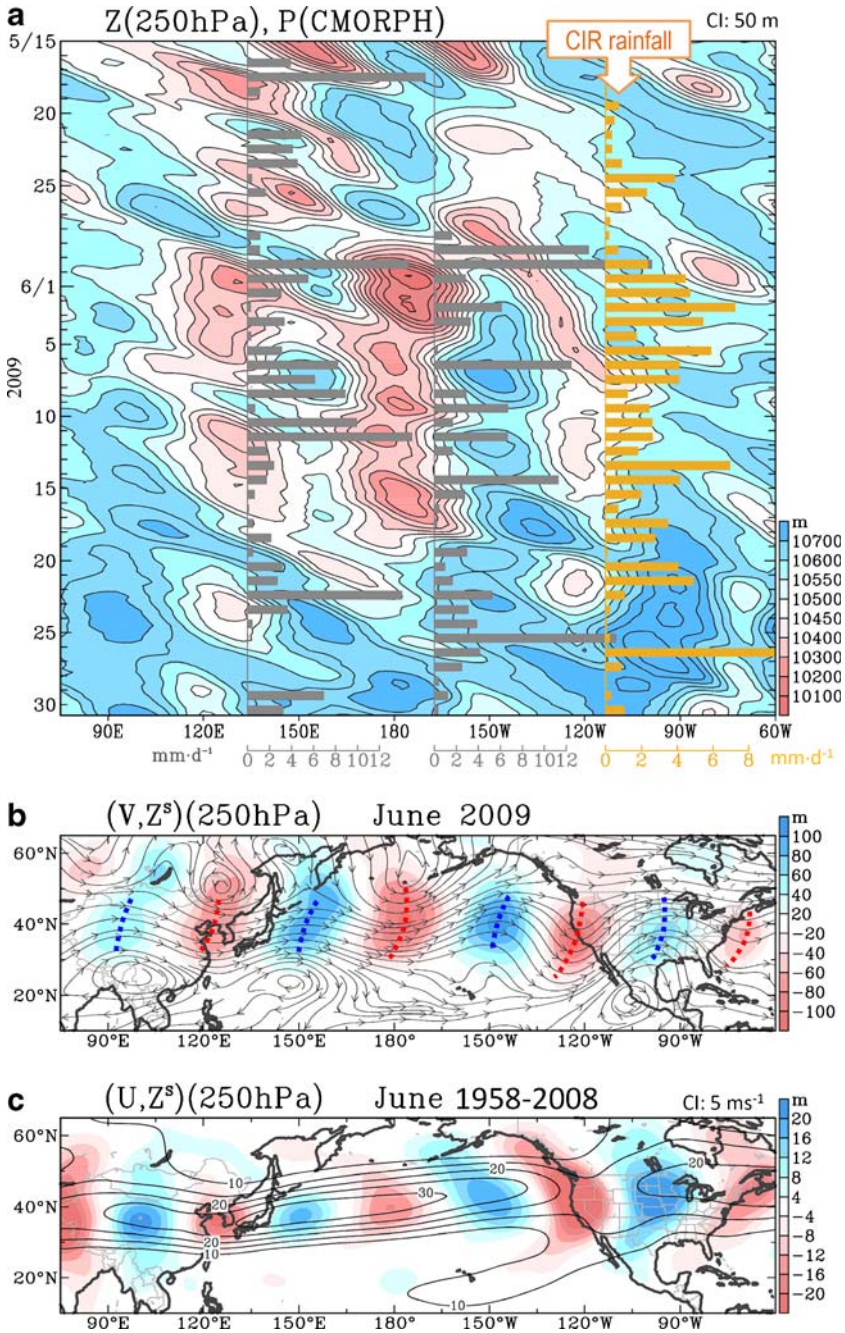

Fig. 2 **a** Longitude–time diagram of 300-hPa geopotential height averaged at 40–45° N from 15 May to 30 June 2009, **b** mean 250-hPa streamlines and the short-wave regime geopotential height (*shadings*) in June 2009 marked with trough (*red*) and ridge (*blue*) lines, and **c** long-term (1958–2008) mean 250-hPa zonal wind (*contours*) and the short-wave regime geopotential height (*shadings*; see text) in June. All fields were based on the NCEP reanalysis. In **a**, the 3-h CMORPH precipitation were accumulated for daily averages (histograms) at 130–140° E, 170–160° E, and the CIW (110–100° W) with the scale at the *bottom*

regime follows that revealed in Branstator (2002) and Ding and Wang (2005) and, therefore, depicts the stationary troughs/ridges that are closest to the wavelength of the circumglobal teleconnection. The climatic short-wave train at 250 hPa (shadings in Fig. 2c) extends from Eurasia to North America along the mean jet stream and is apparently trapped in the jet. The distinct short-wave trough over the West Coast reflects the spring trough that contributes to the CIW rainfall. Moreover, the phase of this climatic short-wave train is strikingly coherent with the phase of the June 2009 short-wave train, as depicted by the filtered geopotential height within the same short-wave regime (shadings in Fig. 2b). Their phase lock indicates that this climatic short-wave train was substantially amplified during June 2009.

To depict the circumglobal teleconnection pattern, the 250-hPa stream function fields (ψ) of NCEP and ERA in June from 1958 to 2008 were spatially filtered with zonal wave numbers 5 and greater and denoted as ψ^S; the year 2009 was omitted to achieve an independent comparison. An empirical orthogonal function (EOF) analysis (e.g., van den Dool 2007) was subsequently applied on the 250-hPa ψ^S within the domain of Fig. 3. Note that the circumglobal teleconnection pattern could be revealed through various

ways, such as one-point regression and correlation analyses as used in Branstator (2002) and Ding and Wang (2005). Here, we adopted a combined method of EOF with spatial filtering in order to objectively extract signals of the short-wave trains while excluding any interference from the more prominent, longer-wave climate modes such as the PNA pattern (i.e., wave numbers 1–3) and the Arctic Oscillation (AO; i.e., annular mode) which would otherwise dominate in the EOF analysis. This method also creates indices of the circumglobal teleconnection based solely on the circulation itself, thereby providing a more independent analysis from other variables (e.g., precipitation) than the regression method.

As shown in Fig. 3a, the first eigenmode (EOF1; 25.5%) depicts a pronounced short-wave train along 40° N that is well in phase with the trough/ridge systems as in 2009, as illustrated by the superimposed trough/ridge lines of 2009 adopted from Fig. 2b. The ψ^S patterns of NCEP (contours) and ERA (shadings) are nearly identical and their coefficients are highly correlated (Fig. 3a, right), indicating a strong agreement between the two datasets. The agreement also signals that the EOF1 pattern, which does not include the year2009 but nonetheless resembles the June 2009 short-wave train, is a prominent mode of the midlatitude circulation variability. Superimposing the USU precipitation anomalies with the EOF1 coefficient (Fig. 3a, right) shows that the precipitation tends to increase (decrease) in association with positive (negative) phases of the EOF1 short-wave train. The correlation coefficient between the USU precipitation and EOF1 is a significant 0.63 for NCEP (0.61 for ERA), as shown in Fig. 3c. These results altogether portray a close association between the June rainfall in CIW and the circumglobal teleconnection.

The EOF2 wave pattern (Fig. 3b) is quadrature phase shifted from the EOF1 wave pattern, suggestive of zonal shifting in the trough/ridge positions of the climatic short-wave train. The EOF2 coefficients of NCEP and ERA are also consistent, but this mode does not correlate with the CIW precipitation (Fig. 3c). To examine possible relationships between the short-wave trains and the major climate modes, the EOF1 and EOF2 coefficients and the USU precipitation were correlated with ENSO (as the December–February NINO3.4 index) and the June indices of NINO3.4, Southern Oscillation, AO, and North Atlantic Oscillation, all of which were based on the NOAA CPC operational monitoring indices.[2] As shown in Fig. 3c, no significant correlation coefficients were found, except for AO which correlates with both the EOF1 short-wave train and the USU precipitation at the 95% confidence level. Ding and Wang (2005) have also noted a statistically significant correlation between the circumglobal teleconnection and AO in June, though no dynamical explanation was provided. In this study, we made no attempt in exploring the potential connection between the short-wave train and AO.

The maintenance mechanism for precipitation associated with the short-wave train was examined through a modified water vapor budget and the mass flux circulation. In view of the marked agreement between NCEP and ERA, the following analysis was performed on the ensemble of these two datasets. By applying the Helmholtz theory, Chen (1985) derived the atmospheric column water vapor flux ($Q = \frac{1}{g}\int_{ps}^{300\,\mathrm{hPa}} Vq \times dp$; q is specific humidity) into the moisture flux stream function (ψ_Q; rotational) and the moisture flux potential (χ_Q; divergent), defined respectively as:

$$\psi_Q = \nabla^{-2}\left(\vec{k} \times \nabla \times Q\right) \tag{1}$$

and

$$\chi_Q = \nabla^{-2}(\nabla \times Q). \tag{2}$$

Since only the divergent component of the water vapor flux $\left(\mathbf{Q}_\mathrm{D} = \nabla\chi_Q\right)$ directly participates in the precipitation process, for the climate variability (Δ), one may obtain:

$$\Delta(\nabla \times Q_\mathrm{D}) = \Delta\left(\nabla^2\chi_Q\right) \approx \Delta P \tag{3}$$

where ΔP is the precipitation anomalies, neglecting the evaporation (e.g., Wang and Chen 2009). The short-wave train that characterized the June 2009 circulation was constructed by the differences of composite ψ_Q and χ_Q between the high-index and low-index years of the EOF1 coefficient (Fig. 4; years given in the caption). Here, the high-index and low-index years were determined by values of the EOF1 coefficient above and below its 0.8 standard deviation, respectively. Similar as in Fig. 3, both ψ_Q and χ_Q were filtered by zonal wave numbers 5 and greater, herein $\Delta\psi_Q^S$ and $\Delta\chi_Q^S$.

The composite pattern of $\Delta\psi_Q^S$ (Fig. 4a) delineates a robust short-wave train along 40° N with a cyclonic cell over the US West Coast. The$\Delta\chi_Q^S$ cells are 90° phase shifted from $\Delta\psi_Q^S$, with convergence (divergence) of water vapor flux coupled to the east (west) of the cyclonic circulations. The contribution of the spatial amplitudes of $\Delta\psi_Q^S$ and $\Delta\chi_Q^S$ to the unfiltered circulation anomalies are 68% and 27%, respectively. Despite its seemingly small contribution, the $\Delta\chi_Q^S$ pattern is clearly in phase with the global precipitation anomalies (Fig. 4b; constructed by UDel over land and GPCP over ocean) that reveal a distinct waveform pattern: along the short-wave train, water vapor flux consistently converges toward positive (diverges from negative) precipitation anomalies east (west) of the cyclonic

[2] The CPC climate indices are provided at ftp://ftp.cpc.ncep.noaa.gov/wd52dg/data/indices/tele_index.nh.

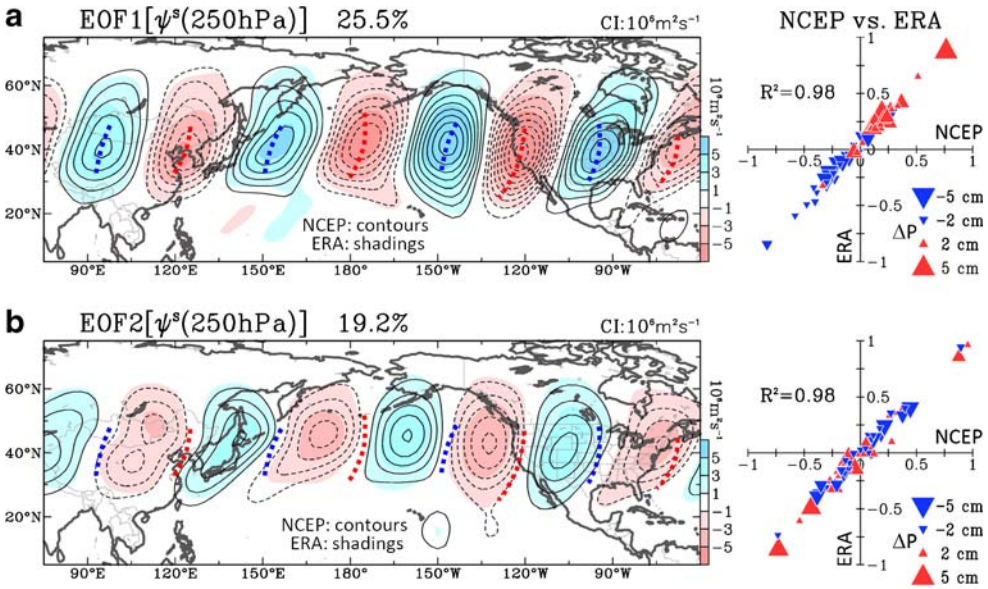

c

	ENSO	NINO3·4	SOI	AO	NAO	P(USU)
P(USU)	0.04	−0.10	0.15	−0.32	−0.14	
EOF1(NCEP)	0.09	0.02	0.00	−0.38	−0.19	0.63
EOF1(ERA)	0.17	−0.02	−0.01	−0.35	−0.10	0.61
EOF2(NCEP)	0.05	−0.07	0.03	0.15	0.16	−0.04
EOF2(ERA)	0.04	−0.06	0.02	0.04	0.18	0.04

Fig. 3 **a** EOF1 and **b** EOF2 of the short-wave stream function at 250 hPa derived from NCEP (*contours*; zeros omitted) and ERA (*shadings*) for 1958–2008, added with the trough and ridge lines from Fig. 2b. The coefficients between NCEP and ERA are shown in the scatter diagrams to the *right* with the scatters showing the USU precipitation anomalies (*triangles*; scales given at the *lower right*). **c** Correlation coefficients of EOF1 and EOF2 and the USU precipitation with various climate indices for 1958–2008. Values that are significant at the 95% (99%) confidence level are shown in *purple* (*red*)

$\Delta\psi_Q^S$ cells. This feature satisfies the precipitation maintenance process as described in Eq. 3. The CIW is situated in the southerly section of the water vapor flux (Fig. 4a) with a convergence center of $\Delta\chi_Q^S$ covering the positive precipitation anomalies (Fig. 4b). Note that the area of positive precipitation anomalies in the CIW also coincides strongly with the June 2009 precipitation pattern in Fig. 1.

The kinematic structure of the short-wave train is shown in Fig. 4c by the cross-sections of the differences of composite geopotential height and mass flux circulation averaged within 40–45° N. The short-wave train exhibits an equivalent barotropic structure with vertically uniform phases, consistent with the previous observations (e.g., Lau and Weng 2002; Branstator 2002). Such a structure is likely formed by balances between absolute vorticity advection and vortex stretching in the upper troposphere and between planetary vorticity advection and vortex stretching in the lower troposphere (Chen 2002). The opposite polarity of vortex stretching in the upper and lower troposphere is balanced by ascending (descending) motion east (west) of the cyclonic cells through mass continuity, thereby creating a dynamically maintained mass flux circulation. The atmospheric column precipitable water (unfiltered) increases correspondingly with converging $\Delta\psi_Q^S$ in the cyclonic vorticity advection regions and, accompanied by the ascent, should enhance precipitation. The CIW is situated in one of such regions under a substantial ascending branch (Fig. 4c; arrow indicated). The consecutive rainfall events in the CIW during June 2009, as shown in Fig. 2a, appear to form by such short-wave train dynamics.

The reasons why the CIW precipitation anomaly of June 2009 was so extreme may be manifold. It was found that the CIW precipitation features robust cyclic signals with a 10- to 20-year frequency (Hidalgo and Dracup 2003; Wang et al. 2009a). Such cyclic signals are discernable in the June precipitation at USU (Fig. 5) as well. Wang et al. (2009b) identified a quadrature-phase modulation of the Pacific quasidecadal oscillation (PQDO) on the CIW precipitation: During the years when the PQDO transitions from a warm phase into a cool phase, a cyclonic circulation develops over the Gulf of Alaska and enhances the CIW precipitation. During the cool-to-warm transition phases of the PQDO, an anticyclonic circulation forms in the Gulf of Alaska and subsequently suppresses the CIW precipitation. As indicated by the 9-year low-passed precipitation time series in Fig. 5, June 2009 appears to be within a positive phase of such quasidecadal variations, so a combined effect of the decadal mode (i.e., PQDO) and the interannual mode (i.e., circumglobal teleconnection) on this precipitation event is likely. Meanwhile, a clear uptrend in June precipitation (Fig. 5) may also contribute to the extreme

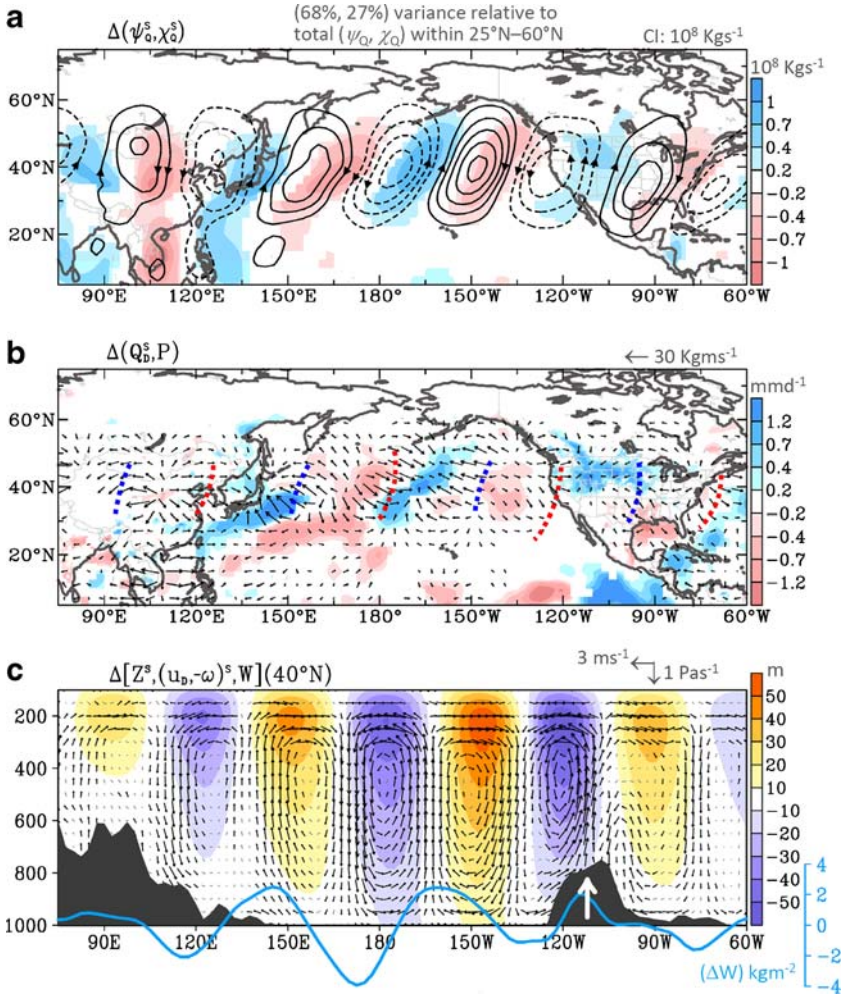

Fig. 4 Differences of composite **a** $\Delta\psi_Q^S$ (*contours*; zeros omitted) and $\Delta\chi_Q^S$ (*shadings*), **b** precipitation (ΔP; *shadings*) and $\Delta\mathbf{Q}_D$ (*vectors*), and **c** longitude–height sections of geopotential height (*shadings*) and mass flux [*vectors* of zonal divergent wind (u_D) and vertical velocity ($-\omega$)] and precipitable water (ΔW) across 40° N between the high-index years (1958, 1967, 1969, 1974, 1975, 1981, 1982, 1992, 1998, 2000, 2002–2004, and 2006) and low-index years (1959, 1961, 1970, 1971, 1973, 1978, 1980, 1986, 1988, 1990, 1991, 1994, 1996, 2001, and 2007) of EOF1. Data are the ensemble of NCEP and ERA. Except for ΔP and ΔW, all fields were spatially filtered with zonal wave numbers 5 and greater. *Shadings* in **a** and **b** and *dark vectors* in **b** and **c** represent values that are significant at the 95% confidence level from a *t* test. The trough/ridge lines of Fig. 2b are added in **b**. The *white arrow* in **c** indicates the CIW

CIW rainfall in 2009. The role of these different climate modes on the precipitation anomalies in the CIW will require a quantitative analysis to reveal.

4 Summary and discussion

Statistical and dynamical evidences in this study suggest that the circumglobal teleconnection has a profound impact on early summer precipitation in the CIW. The distinct short-wave train of the June 2009 circulation pattern is likely an amplification of the stationary short-wave train embedded in the jet stream (cf. Fig. 2c). This result sheds light on the abnormal, yet recurrent, June precipitation events recorded in the CIW (cf. Fig. 5). It is known that precipitation variations in the CIW lack a direct association with ENSO and other tropical Pacific forcings because the CIW is situated in the marginal zone of the prominent north–south precipitation pattern driven by ENSO (e.g., Dettinger et al. 1998) where any positive influences from El Niño/La Niña are likely canceled out by negative influences (Wang et al. 2009a). On the other hand, the CIW precipitation is very sensitive to circulation patterns over the West Coast (Wang et al. 2009b) where the spring trough is located. This character coincides with the fact that the circumglobal teleconnection pattern, which strongly modulates the spring trough, is unrelated to ENSO (Branstator 2002; Ding and Wang 2005).

We also identified a new prevailing mode of the circumglobal teleconnection in addition to that revealed in Ding and Wang (2005). To compare with their results, we constructed the regression patterns of eddy stream function (unfiltered) and precipitation anomalies with the EOF2 coefficient obtained from the analysis in Fig. 3b. The constructed EOF2 patterns (Fig. 6a) are fairly consistent with the circumglobal teleconnection and precipitation patterns as depicted in Ding and Wang (2005; Fig. 6b; adopted from their Fig. 7a). In this case, the short-wave train is linked to rainfall variations in northern India and possibly in the Great Plains as well (Weaver and Nigam 2008), but not in the CIW as indicated by the lack of significant precipitation anomalies in the CIW (Fig. 6a). Thus, these observations point to two possible modes of the summer circumglobal teleconnection: amplification/weak-

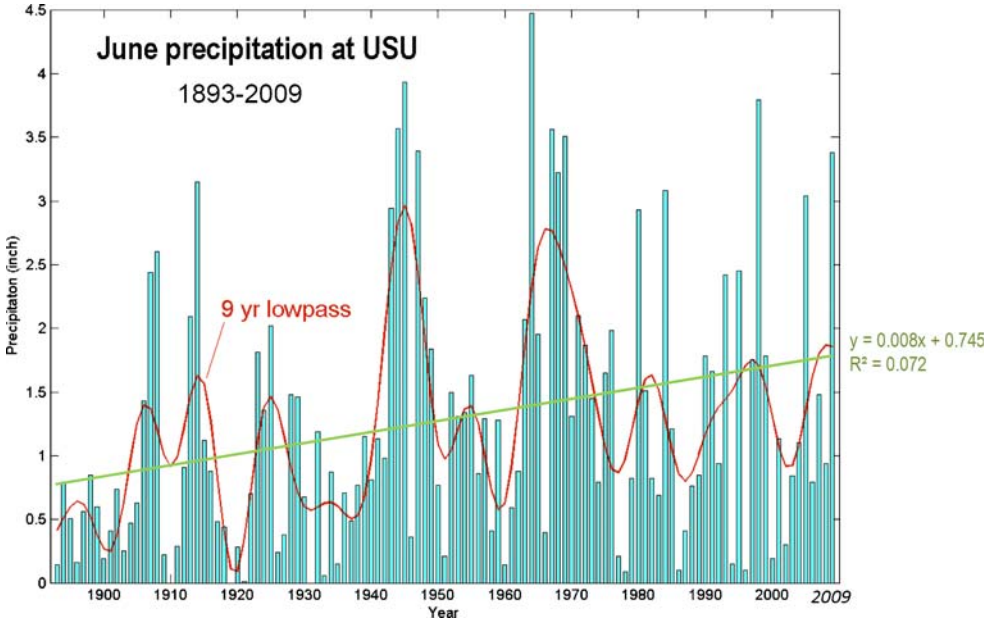

Fig. 5 June precipitation at USU (histogram) from 1893 to 2009, added with the 9-year low-passed time series (*red line*) and linear trend (*green line*)

ening of the climatic short-wave train as in this study, and zonal shifting of the climatic short-wave train as in Ding and Wang (2005). Nevertheless, their forcing mechanism remains an open question.

Based on the waveguide theory in which propagating Rossby waves are confined to a narrow/belt path such as the jet region (Hoskins and Ambrizzi 1993), any disturbances along the jet stream may either trigger or enhance wave responses downstream (Branstator 2002). For instance, Kurihara and Tsuyuki (1987) found that changes in summer precipitation and circulation around Japan can induce Rossby wave propagations across the North Pacific to the Gulf of Alaska. The marked precipitation and circulation anomalies east of Japan in Fig. 4 seem to

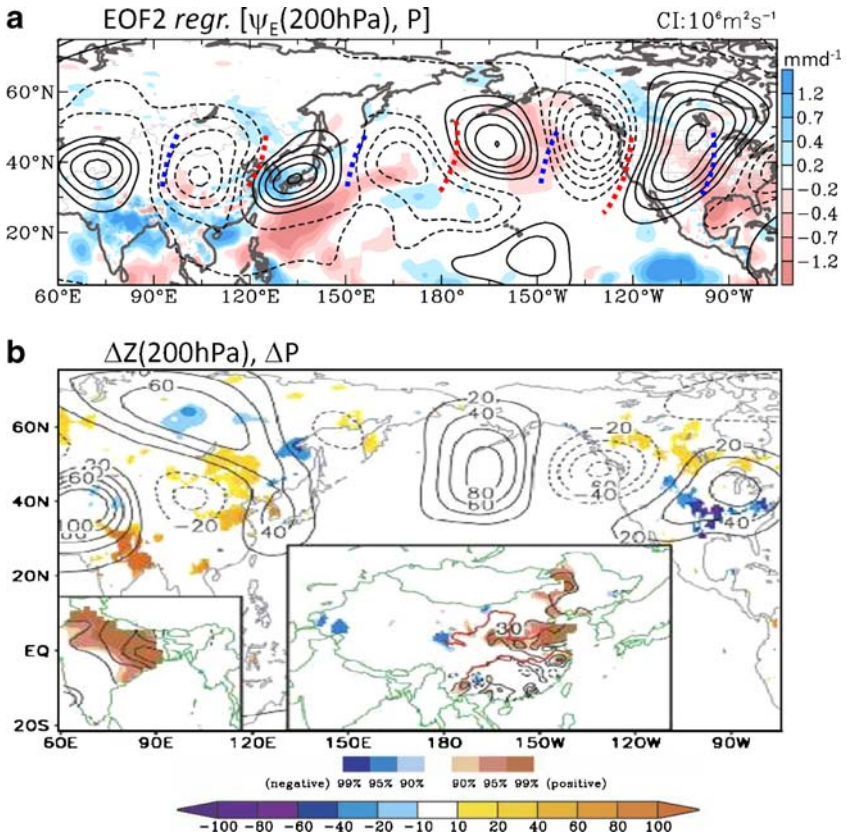

Fig. 6 **a** Regression patterns of the 200-hPa eddy stream function (*contours*; zeros omitted) and the GPCP/UDel precipitation (*shadings*) with EOF2 from 1958 to 2008, added with the trough/ridge lines as those in Fig. 2b and **b** the June circumglobal teleconnection pattern and its associated precipitation anomalies as depicted in Ding and Wang (2005; adopted from their Fig. 7a showing the composite 200-hPa geopotential height and rainfall anomalies). Note the phase coincidence between the two wave trains and the precipitation patterns

support such a forcing mechanism. However, as inferred from the composite precipitation pattern (cf. Fig. 4b), each diabatic heating source/sink along the jet stream could be both a source and a response of the teleconnection wave train, thereby making the determination of initial forcing source difficult. Before its forcing problem can be resolved, the impact of the circumglobal teleconnection on regional climate, as is observed in the CIW, deserves further analysis.

Acknowledgements This study was supported by the USDA CSREES-funded Drought Management, Utah Project and by the Utah Agricultural Experiment Station, Utah State University, and approved as journal paper number 8164. XJ acknowledges support by NOAA CPPA program under Award NA09OAR4310191. Discussion with T.-C. Chen regarding the stationary short-wave train was much appreciated.

References

Branstator G (2002) Circumglobal teleconnections, the jet stream waveguide, and the North Atlantic Oscillation. J Clim 15:1893–1910

Barnston AG, Livezey RE (1987) Classification, seasonality and persistence of low-frequency atmospheric circulation patterns. Mon Weather Rev 115:1083–1126

Chen TC (1985) Global water vapor flux and maintenance during FGGE. Mon Weather Rev 113:1801–1819

Chen TC (2002) A North Pacific short-wave train during the extreme phases of ENSO. J Clim 15:2359–2376

Dettinger MD, Cayan DR, Diaz HF, Meko DM (1998) North–south precipitation patterns in western North America on interannual-to-decadal timescales. J Clim 11:3095–3111

Ding Q, Wang B (2005) Circumglobal teleconnection in the Northern Hemisphere summer. J Clim 18:3483–3505

Hidalgo HG, Dracup JA (2003) ENSO and PDO effects on hydroclimatic variations of the Upper Colorado River Basin. J Hydrometeorol 4:5–23

Higgins RW, Yao Y, Wang XL (1997) Influence of the North American monsoon system on the U.S. summer precipitation regime. J Clim 10:2600–2622

Hoskins BJ, Ambrizzi T (1993) Rossby wave propagation on a realistic longitudinally varying flow. J Atmos Sci 50:1661–1671

Huffman GJ et al (1997) The Global Precipitation Climatology Project (GPCP) combined precipitation dataset. Bull Am Meteorol Soc 78:5–20

Joyce RJ, Janowiak JE, Arkin PA, Xie P (2004) CMORPH: a method that produces global precipitation estimates from passive microwave and infrared data at high spatial and temporal resolution. J Hydrometeorol 5:487–503

Kalnay E et al (1996) The NCEP/NCAR 40-year reanalysis project. Bull Am Meteorol Soc 77:437–470

Kurihara K, Tsuyuki T (1987) Development of the barotropic high around Japan and its association with Rossby wave-like propagations over the North Pacific: analysis of August 1984. J Meteorol Soc Jpn 65:237–246

Lau KM, Weng HY (2002) Recurrent teleconnection patterns linking summertime precipitation variability over East Asia and North America. J Meteorol Soc Jpn 80:1309–1324

Lau KM, Kim KM, Lee JY (2004) Interannual variability, global teleconnection and potential predictability associated with the Asian summer monsoon. In: Chang CP (ed) East Asian Monsoon. World Scientific, Singapore, 564 pp

Legates DR, Willmott CJ (1990) Mean seasonal and spatial variability in gauge-corrected, global precipitation. Int J Climatol 10:111–127

Takaya K, Nakamura H (2001) A formulation of a phase-independent wave-activity flux for stationary and migratory quasigeostrophic eddies on a zonally varying basic flow. J Atmos Sci 58:608–627

Uppala SM et al (2005) The ERA-40 re-analysis. Q J R Meteorol Soc 131:2961–3012. doi:10.1256/qj.04.176

Uppala SM, Dee D, Kobayashi S, Berrisford P, Simmons A (2008) ECMWF Newsletter 115:12–18

van den Dool H (2007) Empirical methods in short-term climate prediction. Oxford University Press, Oxford, 215 pp

Wallace JM, Gutzler DS (1981) Teleconnections in the geopotential height field during the Northern Hemisphere winter. Mon Weather Rev 109:784–812

Wang SY, Chen TC (2009) The late spring maximum of rainfall over the United States Central Plains and the role of the low-level jet. J Clim 22:4696–4709

Wang SY, Gillies RR, Jin J, Hipps LE (2009a) Coherence between the Great Salt Lake level and the Pacific quasi-decadal oscillation. J Clim. doi:10.1175/2009JCLI2979.1

Wang SY, Gillies RR, Jin J, Hipps LE (2009b) Recent rainfall cycle in the Intermountain Region as a quadrature amplitude modulation from the Pacific decadal oscillation. Geophys Res Lett 36: L02705. doi:10.1029/2008GL036329

Wang SY, Gillies RR, Takle ES, Gutowski WJ (2009c) Evaluation of precipitation in the Intermountain Region as simulated by the NARCCAP regional climate models. Geophys Res Lett 36: L11704. doi:10.1029/2009GL037930

Weaver SJ, Nigam S (2008) Variability of the Great Plains low-level jet: large-scale circulation context and hydroclimate impacts. J Clim 21:1532–1551

Yang S, Lau KM, Kim KM (2002) Variations of the east Asian jet stream and Asian–Pacific–American winter climate anomalies. J Clim 15:306–325